Soft Matter

Cite this: *Soft Matter*, 2011, **7**, 4397

www.rsc.org/softmatter

PAPER

Chain extension in electrospun polystyrene fibres: a SANS study

Saeed D. Mohan,[a] Geoffrey R. Mitchell[abc] and Fred J. Davis*[a]

Received 7th December 2010, Accepted 15th February 2011
DOI: 10.1039/c0sm01442g

Small angle neutron scattering techniques were used to quantify the size and shape of the chain conformation in electrospun fibres of atactic polystyrene prepared from solutions in methyl ethyl ketone. Aligned arrays of fibres were collected onto a rotating collector with tangential velocity varying between 0 ms^{-1} and ~15 ms^{-1}. The measured radii of gyration of the polystyrene chains were found to be slightly higher than that expected for samples prepared from solutions in the concentrated regime. The ratio of the radius of gyration parallel and perpendicular to the chain axis was found to be ~1.05 in contrast to the substantial macroscopic shape transformation intrinsic to electrospinning. When the tangential velocity of the rotating collector was greater than the flight velocity of the fibres (*ca.* 4 ms^{-1}), a further extension of the polymer chains was observed with a ratio of the radii of gyration increasing to 1.20 at the highest collector speeds. It is proposed that the heterogeneous processes involved, particularly solvent evaporation and the formation of a polymer skin during electrospinning play a significant role in determining the level of molecular anisotropy in the fibres.

Introduction

Electrospinning involves the generation of nano- and micro-scale polymer fibres by means of applying an electric field to droplets of a polymer solution passed through a needle tip.[1] The fibres produced by the electrospinning process are of great interest for applications including filtration,[2] catalysts,[3] drug delivery[4] and tissue engineering.[5] Under the direct influence of the Coulombic electric forces, a small droplet of the solution will become charged and as a consequence its shape will become distorted to form a cone-like geometry.[6] For effective electrospinning, the polymer solution must be at a concentration which contains chain entanglements,[7] and typically involve a polar, high dielectric solvent. On exposure to a sufficiently high electric field, the droplet is distorted and a jet of polymer solution is ejected resulting in a fine fibre being deposited on the collector electrode. Under such circumstances the bulk of the solvent may be removed from the polymer in a fraction of a second. The transformation in terms of geometric aspect ratio from the droplet to the final fibre may be as high as 60 000.[8] Under such conditions, a quantitative knowledge of the shape and dimensions of the polymer chain trajectories in the final fibre is critical to understanding the molecular reorganisation processes in the electrospinning procedure. We have set out to use the particular power of small-angle neutron scattering (SANS) techniques coupled with isotopically labelled polymer chains to reveal and evaluate the radius of gyration parallel and perpendicular to the fibre axis of electrospun fibres.

In terms of the evaluation of the development of molecular level structure, electrospinning has proved particularly challenging. The development of structure is most easily observed in systems which exhibit crystallinity, for example, Tosaka *et al.* have studied orientation in the skin layer of electrospun isotactic polystyrene using transmission electron microscopy[9] and Bellan and Craighead have utilised Raman to probe the orientation in crystalline samples of Nylon-6.[10] However, for many techniques, a single fibre strand is impracticable; a bundle of fibres with the same fibre axis is required to give a satisfactory signal to noise ratio. There are several methods that have been used to obtain aligned fibres, but the most widely used are a rotating collector[11,12] and a parallel electrode arrangement.[13] Several methods have been attempted to measure anisotropy in the fibre structures although the small scale of the fibre diameter makes this challenging on all but the larger fibres. For example infra-red spectroscopy has been used by Lee *et al.*[14]and by Wang *et al.*[15] to reveal a certain stretching of the polymer chains. Birefringence has been used to study polyacrylonitrile fibres,[16] and atactic polystyrene fibres.[17] Such studies indicate that the chains are partially extended by electrospinning but particularly for samples collected with a rotating collector, this orientation may be induced by the mechanical extension of the fibres, particularly at high collector speeds.[12]

In our investigations we have focused on atactic polystyrene as it is a completely amorphous polymer and we are able to probe

[a]*Polymer Science Centre, University of Reading, Whiteknights, Reading, UK. E-mail: f.j.davis@reading.ac.uk; Fax: +44 (0)118 378; Tel: +44 (0)118 378 8455*
[b]*Centre for Advanced Microscopy, University of Reading, Whiteknights, Reading, UK*
[c]*Centre for Rapid and Sustainable Product Development, Institute Polytechnic of Leiria, Rua de Portugal, 2430-028 Marinha Grande, Portugal. E-mail: g.r.mitchell@reading.ac.uk*

the molecular level reorganisation without the complication of partial crystallisation. Atactic polystyrene also provides the advantage that the small-angle neutron scattering behaviour of this polymer is well understood. For example, the deformation of polymer chains of hot stretched polystyrene has been observed using SANS[18–20] and the radius of gyration of the polymer chains measured parallel and perpendicular to the direction of extension. The polymer chains were observed to follow an affine deformation. Furthermore, Wignall and Melnichenko have gathered results from various works to show that amorphous glassy or molten polystyrene exhibits an unperturbed chain dimension,[21] and that the radius of gyration of the polymer chain can be simply related to the (weight average) molecular weight M_w (in fact the relationship is $R_g = 0.275\ M_w^{0.5}$). In the account that follows we employ this methodology, together with variations in collector conditions to monitor the polymer backbone anisotropy in electrospun polystyrene fibres, and in particular to decouple effects caused by the mechanical force induced by the collector, and the anisotropy inherent to electrospinning.

Experimental

Per-deuterated and per-hydrogenated atactic polystyrenes were prepared as follows: purified styrene (9.0 g, 86.41 mmol) was taken in a Pyrex polymerization tube (fitted with a Young's tap and a protective netting sleeve) along with azobisisobutyronitrile (0.09 g, 0.54 mmol) as an initiator. The monomer and initiator were degassed using the freeze–pump–thaw technique. The tube containing the degassed monomer was placed in a thermostatted water-bath at 55 °C for 24 h. After polymerisation, the glassy solid lump of the polymer was dissolved in dichloromethane (30 ml) and precipitated in cold, stirred methanol (400 ml). The polymer was purified by dissolving in dichloromethane (10 ml), re-precipitating in cold methanol (300 ml), and then drying *in vacuo* at 70 °C.

Molecular weight distributions were measured using GPC with tetrahydrofuran as the solvent and polystyrene standards. The deuterated atactic-polystyrene sample gave M_w of 400 000 g mol^{-1} and M_n of 110 000 g mol^{-1}, the hydrogenated atactic polystyrene gave M_w of 325 000 g mol^{-1} and M_n of 116 000 g mol^{-1}. The polymers used for electrospinning were dissolved in methyl ethyl ketone (butanone, MEK) using a Buhler shaker for 24 hours prior to electrospinning. The electrospinning apparatus was arranged in a horizontal configuration. Solutions for electrospinning were placed inside a 5 ml Luer lock glass syringe with a 0.41 mm internal diameter needle mounted in a syringe pump. A Glassman High Voltage Supply provided a voltage of 5–20 kV on the needle with respect to the grounded electrode. An auxiliary electrode made from copper was also attached to the needle at the same potential as the needle.

Two collector electrode assemblies were used both situated at a variable distance from the needle tip. One electrode system consists of a rotating cylinder 7 cm long with a radius of 1.6 cm; the electrode surface was a removable aluminium foil. The surface tangential speed of the collector could be varied from 0 ms^{-1} to ~15 ms^{-1}. The second electrode system consisted of a pair of parallel aluminium electrodes separated by 5 cm. All samples were left to dry for a minimum of 24 hours to remove any remaining solvent which was confirmed using NMR analysis, with a Bruker Avance III 400 MHz Spectrometer with deuterated chloroform as the solvent. The NMR analysis showed that the fibres as spun contained ~1% w/w of solvent which reduced to ~0.2% after 3 hours in the laboratory atmosphere. After 6 hours there was no detectable level of solvent present in the fibres.

The electrospun fibres were examined using a Cambridge Instrument 360 Scanning Electron Microscope. All samples were coated with gold prior to examination. Fibre diameters were sampled by overlaying a grid on the SEM image of the collected fibres; several fibres were randomly selected from each grid square, thereby obtaining an unbiased representation of the fibre diameter distribution. The details of the cross-section of the fibres were obtained by mounting the fibres in an epoxy resin and left to set at 60 °C for 48 hours. A Reichert-Jung Ultracut E ultramicrotome equipped with a glass knife was used to prepare a surface normal to the fibre axis.

SANS experiments were performed using the LOQ small angle diffractometer[22] at the ISIS Pulse Neutron Source (STFC facility Rutherford Appleton Laboratory, Didcot, UK) with a 12 mm diameter incident beam. A wavelength, λ, range of 2.2 Å–10 Å was employed giving a scattering vector range, $|Q|$ of 0.009 Å^{-1}–0.25 Å^{-1} where $|Q| = 4\pi\sin\theta/\lambda$ and 2θ is the scattering angle. Electrospun fibre samples were removed from the collector electrode and mounted on the sample holder rack on the LOQ instrument using an aluminium foil. Scattering data were accumulated for each sample for ~60 minutes in order to obtain a good signal to noise ratio. Scattering data were collected on the two-dimensional ORDELA area detector. The data were corrected for the absorption and scattering from the sample container[23] and converted to an absolute scale using measurements on known polystyrene blends and established procedures.[24] For part of the analysis, the 2-d data were reduced to one-dimensional differential scattering cross-section $((d\Sigma/d\Omega)(Q))$, as a function of $|Q|$ in order to analyse data parallel and perpendicular to the fibre axis. Functions were prepared by averaging the data from $\alpha = -30°$ to 30° and $\alpha = 60°$ and 120° and symmetrical related angle where α is the angle between the fibre axis and Q. Data analysis was performed in a non-linear least squares data fitting program (FISH).[25] The evaluation of the incoherent scattering was incorporated into the data fitting method.

Results and discussions

The nature of the fibres produced by the electrospinning technique depends crucially on the operating parameters. After a series of exploratory experiments using solutions of hydrogenated polystyrene, the following conditions were found to produce continuous non-beaded fibres on a reproducible basis: solution concentration 27% w/w polystyrene in MEK, flow rate 0.13 ml min^{-1}, potential 10 kV, needle to collector distance 20 cm. These were used to prepare samples for SANS measurements using a 1 : 1 mixture of perdeuterated polystyrene and perhydrogenated polystyrene.

Fig. 1a shows an SEM micrograph of electrospun fibres that were prepared using the static parallel plate collector system. The SEM image shows that the fibres are bead free and around 13 μm in width. Closer inspection shows that the fibres do not possess

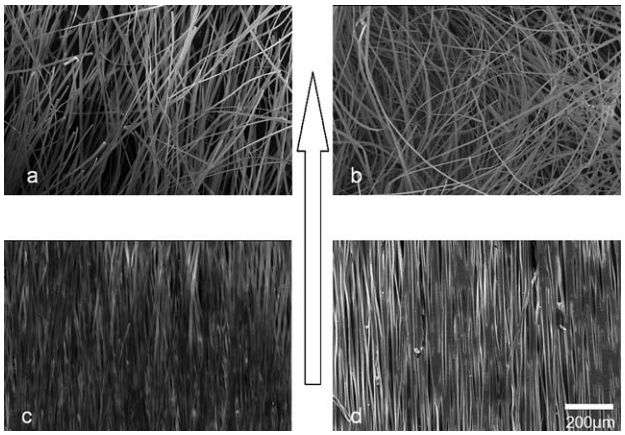

Fig. 1 SEM micrographs of fibres spun using (a) static parallel plates and (b–d) a rotating collector with tangential speeds of (b) 0.8 ms^{-1}, (c) 5.0 ms^{-1}, (d) 14.6 ms^{-1}. The arrow indicates the direction of rotation for b–d and for a, the arrow indicates the direction normal to the plates.

a circular, but a rather flat cross-section. Such flat cross-sections have been observed in a number of studies and are thought to arise when a skin forms on the fibre, trapping some solvent; subsequent solvent loss leads to a collapse of the fibre to a flat structure.[26] We will analyse the cross-sections in more detail later, but for an initial model the width measurements relate to the larger of the two cross-section dimensions. The fibres are aligned preferentially around a common direction, namely about the vertical axis on the page, which corresponds to the inter-electrode vector in the collector assembly. However, there is some misalignment present.

Fig. 1b–d show SEM images of electrospun fibres that were collected using a rotating collector at tangential speeds of 0.8 ms^{-1}, 5.0 ms^{-1} and 14.6 ms^{-1}. In each case the rotation direction is vertical on the page, and the fibres show a similar flat cross-section. It is clear that the level of common alignment of the fibres in Fig. 1c and d is higher than that in Fig. 1a. With increasing speed there is a corresponding increase in the alignment levels. Fig. 2 shows a plot of the mean fibre width as a function of the collector tangential speed. The inset shows the fibre width distribution for the fibres collected onto the parallel plates. Each width distribution (see inset) was fitted with a normal distribution and the full width at half maximum of each distribution is plotted in Fig. 2 as a bar. With increasing speed of the rotating collector the mean width reduces, and the distribution of fibre widths narrows. Similar results in terms of a narrowing of fibre distribution with increasing collector speeds were observed by Edwards *et al.*[12]

Fig. 3 shows the mean angle obtained from a distribution $D(\phi)$ of the angle each fibre made with the rotation direction measured from the SEM images. The results show that as the collector velocity increased the fibres became increasingly aligned with the rotation direction; this reached a plateau at 5 ms^{-1}. Using each distribution, $D(\phi)$, the orientation parameter $\langle P_2 \rangle_f$ was calculated, where $\langle P_2 \rangle_f = \langle (3\cos^2 \phi - 1)/2 \rangle$. $\langle P_2 \rangle_f = 1$ corresponds to a completely aligned system and $\langle P_2 \rangle_f = 0$ corresponds to a random fibre matt. Fig. 3 shows that the value of $\langle P_2 \rangle_f$ increases steadily with increasing collector velocity and reaches a plateau value of *ca* 0.95 at a tangential velocity of 5 ms^{-1}. The fibres prepared using the parallel plate electrodes gave $\langle P_2 \rangle_f = 0.65$.

At low collector rotation speeds, the velocity of the fibres produced by the electrospinning jet is greater than the tangential speed of the collector. As a consequence there is no tension on the fibre, and hence the fibres are wound up with a rather random alignment on the electrode.[12] When the speed of the collector matches that of the jet speed, the fibre axis alignment becomes very high. At higher collector speeds, the windup rate will be higher than the fibre production speed. This differential speed deforms and extends the fibre; this can be observed in the decreasing fibre width. At even higher collector rotation speeds

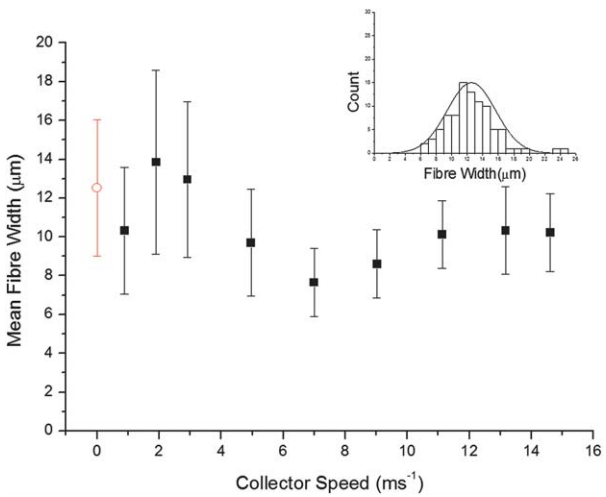

Fig. 2 Variation in the mean fibre width as a function of the tangential collector speed. The sample collected using parallel plates is represented by circle. The bars show the full width half maximum of the width distribution for each set of fibres. The inset shows the distribution of fibre widths for the fibres collected using the parallel plate system.

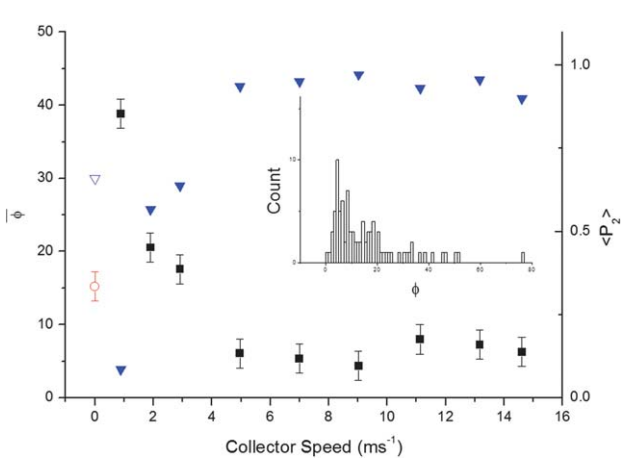

Fig. 3 A plot (■) of the mean angle ϕ from the rotation direction for fibres collected at different collector speeds and (▼) the values of $\langle P2 \rangle$ derived from the angular distribution. The sample collected using parallel plates is represented by the open symbols. The inset shows the distribution of ϕ for the fibres collected using the static parallel plate arrangement.

the stress on the fibre is too high and fibre breakage occurs. This is observed directly during the spinning process to be adjacent to the Taylor Cone. A consequence of this breakage is that the mean fibre width increases slightly as the effective fraction of fibres under tension is reduced. Inspection of Fig. 2 and 3 shows that fibre deformation is initiated at a collector speed of between 3 and 5 ms^{-1}. To check the fibre production velocity, we collected fibres for fixed time periods. From the mass of the fibres produced and the measured fibre cross-section we have estimated that under the conditions employed, the fibre velocity adjacent to the collector as 4.2 ms^{-1} which is consistent with the observations above.

Fig. 4 shows the measured SANS patterns for three of the fibre samples. In each case the rotation direction is vertical on the page. These patterns show the expected patterns for an isotopically labelled mixture in the amorphous state. The vertical and horizontal cross-sections, taken from the SANS pattern for the fibres prepared with a collector velocity of 14.6 ms^{-1}, show the typical fall-off in scattering with increasing values of Q. Fig. 4a shows the scattering for the sample prepared using the parallel electrode collector. Although the scattering is almost the same in all directions, *i.e.* isotropic, there is a small but distinct difference between the scattering with Q parallel to the fibre axis and Q perpendicular to it. These differences increase in Fig. 4b and are mostly easily seen in Fig. 4c. The shape of the scattering is extended along the horizontal axis and compressed on the vertical axis as is expected for a random polymer chain extended along the fibre axis. The degree of anisotropy reflects the level of chain extension.

The scattering from the fibres will exhibit uniaxial symmetry and so we can describe the level of anisotropy in the scattering pattern, $S(|Q|,\alpha)$, using the coefficients of a series of even ordered Legendre polynomials P_{2n}. Here we restrict our attention to the second term which can be evaluated using:

$$\langle P_2\rangle_o = \frac{\int_0^{90} S(|\underline{Q}|,\alpha) P_2(\cos\ \alpha) \sin\ \alpha\, d\alpha}{\int_0^{90} S(|\underline{Q}|,\alpha) \sin\ \alpha\, d\alpha} \quad (1)$$

with equivalent expressions for the 3 symmetry related quadrants of the scattering pattern. The level of molecular anisotropy $\langle P_2\rangle$ can be obtained using the methodology based on the Legendre Addition Theorem:[27,28]

$$\langle P_2\rangle = \frac{\langle P_2\rangle_o}{P_2^m} \quad (2)$$

where $\langle P_2\rangle_o$ is the coefficient obtained from the experimental scattering and P_2^m is the coefficient for the scattering from a perfectly aligned chain. For an extended chain the scattering will be confined to the equatorial plane and hence $P_2^m = -0.5$.[27] We have used this approach and the scattering between $Q = 0.02$ and 0.1 to obtain values of $\langle P_2\rangle$ for each of the electrospun fibre samples and these are plotted in Fig. 5 as a function of the collector tangential speed. We have also plotted the result for the sample prepared using the parallel electrode system. The value of $\langle P_2\rangle$ for that sample is broadly similar to that for the sample prepared with a collector velocity of 3 ms^{-1}. Those prepared at higher velocities exhibit values for $\langle P_2\rangle \sim 0.1$.

The SANS scattering observed is the convolution of the scattering from a fibre with the orientation distribution $D(\phi)$ describing the alignment of the fibres in the neutron scattering sample. As a consequence the orientation parameters shown in Fig. 5 also include the effect of the fibre angular distribution.

The advantage of expressing the orientation using spherical harmonics is that the deconvolution required to obtain the orientation within a fibre $\langle P_2\rangle_{sf}$ can also be obtained using the methodology of the Legendre Addition Theorem:[27,28]

$$\langle P_2\rangle_{sf} = \frac{\langle P_2\rangle}{\langle P_2\rangle_f} \quad (3)$$

We have plotted the values obtained for $\langle P_2\rangle_{sf}$ using eqn (3) and the data in Fig. 3 and 5 as an additional series of points in

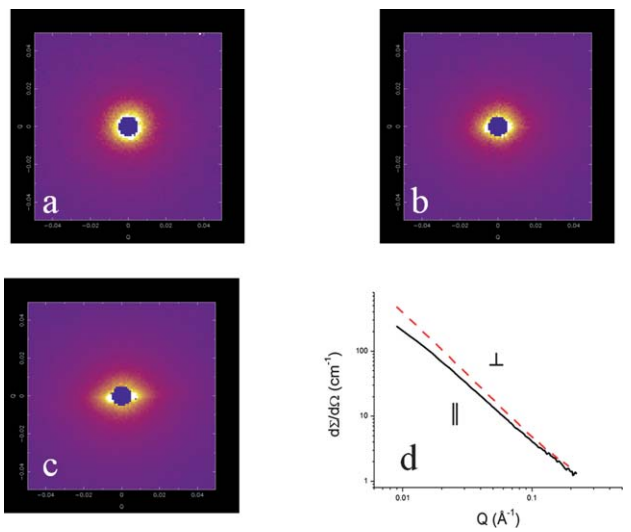

Fig. 4 2-d SANS patterns obtained for fibres collected using (a) static parallel plates, (b) rotating collector with a tangential speed of 5 ms^{-1}, (c) rotating collector with a tangential speed of 14.6 ms^{-1} and (d) the differential scattering cross-sections of the pattern in (c) parallel (solid line) and perpendicular (dashed line) to the rotation direction.

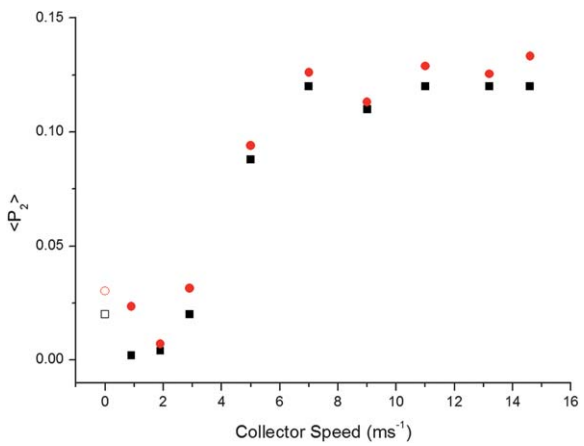

Fig. 5 Orientation parameter $\langle P_2\rangle$ for the polymer chain obtained from the SANS data as a function of the collector speed ■ uncorrected for fibre angular alignment on the electrode ● corrected for the fibre angular alignment on the electrode. The open symbols represent the sample collected with the static parallel plate electrodes.

Fig. 5 (circles). The basic pattern of the orientation parameters *versus* collector speed remains largely the same. At high collector speeds, the fibre alignment is high and so the adjustment is proportionally small. At low collector velocities the adjustment remains small but it is proportionally large. The orientation parameter for the static collector and the low speed collector samples shows values ~0.03. For the sample prepared with a velocity of 2 ms^{-1}, the level of orientation is rather low (Fig. 1b). Intriguingly, in related work[12] and in reports in the literature,[29] at low speeds there seems to be a similar reduction in preferred alignment compared to the static electrode case. We attribute this reduction to the lack of tension on the fibre and hence the randomising effect of the moving collector.

Exploratory studies revealed that the electrospun fibres prepared in this work contained nanovoids. We have evaluated these voids using the SANS from electrospun fibres prepared solely from perdeuterated polystyrene; thus allowing the isolation of the scattering from these feature. We found that the scattering from the voids followed the form:

$$I_{\text{voids}}(Q) = BQ^{-N} \tag{4}$$

where B is a scaling constant and $N = 4$. Further analysis of the SANS data gave spherical nanovoids with a Schultz distribution of radii centred on 130 Å with a polydispersity index of 0.5.

The SANS scattering for a system of labelled polydisperse Gaussian chains is given by:[30]

$$\left(\frac{d\Sigma}{d\Omega}(Q)\right) = \frac{A}{((1+U)y^2)}\left\{y - 1 + (1+Uy)^{-1/U}\right\} \tag{5}$$

where $A = 2x(1-x)V(\Delta\rho)^2$, x is the polymer concentration of the labelled species, V is the volume, R_g is the radius of gyration of the polymer chains, $\Delta\rho$ is the difference in scattering length density, $y = (QR_g)^2/(1+2U)$ and $U = 1 - M_w/M_N$.

We have used non-linear least squares minimisation techniques to fit a combination of these two functions to sections taken through the observed SANS data of the isotopically labelled mixtures parallel and perpendicular to the fibre axis. There are only two variables, R_g and B, all other parameters A, $(\Delta\rho)^2$, x and V are fixed by material properties. For data fitting purposes R_g is initially set to that of the bulk state material and B is 0.

We have applied these procedures to the SANS data recorded for each sample of electrospun fibres and the results for the radius of gyration parallel and perpendicular to the fibre axis are shown in Fig. 6. For these aligned samples there is a larger radius of gyration value parallel to the fibre axis when compared to the perpendicular component indicating an extension of the chain conformation along the fibre axis. In some cases the ratio of R_g parallel to R_g perpendicular is ~1.2. This is the case at the higher collector speeds. For the static electrode case the ratio is ~1.05. Calculation of the isotropic average R_g for the range of collector speeds yields a value of 178 Å. Fig. 6 shows for reference the predicted value of $R_g = 170$ Å for the equivalent polymers in the bulk state based on data obtained from previous investigations on SANS of atactic-polystyrene.[21] The results displayed in Fig. 6 clearly indicate that there is a larger mean R_g for the fibres than that of the equilibrium bulk state material by about 5%. This difference may be due to the expanded nature of the chains in the solution; in this context MEK is a reasonably good solvent.

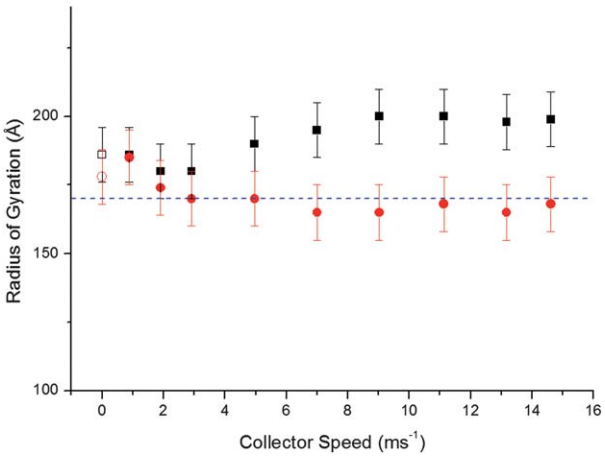

Fig. 6 Radius of gyration of the polymer chains obtained from the SANS data ■ parallel and ● perpendicular to the rotation direction. The open symbols represent the sample collected using the static parallel plate system. The dashed line represents the equilibrium bulk state value calculated using the results given in ref. 21.

The overlap concentration for a polymer solution is given by:

$$\phi^* = \frac{3M_w}{4\pi\rho N_A R_g^3} \tag{6}$$

where ϕ is the volume fraction of the polymer, M_w is the molecular weight of the polymer, ρ is the polymer density and N_A is Avagadro's number. For a polymer in the unperturbed state in solution R_g can be determined from:

$$R_g = KM_w^{\gamma} \tag{7}$$

where K and γ have been evaluated for solutions of polystyrene in MEK to be 1.37×10^{-2} nm and 0.57 respectively.[32] Eqn (7) gives the value for the R_g with this polystyrene at zero concentration to be 214 Å. Using this value and eqn (6), the volume fraction at the overlap concentration is calculated at 0.0154 for a polymer with M_w 400 000 g mol^{-1} or 2.0% w/w concentration. Clearly the concentration used in the electrospinning (27% w/w) is significantly greater. In the semi-dilute regime, *i.e.* above the overlap concentration, scaling theory gives $R_g \approx c^{-\mu}$ ref. 31 although there are some variations in the exponent μ from theory and experiment. Theory suggests that at high concentrations solution will be in a concentrated regime where the state of the polymer is close to that of the equilibrium bulk material. Fig. 7 compares the expected variation of R_g based on the estimates calculated above and the scaling exponent for a good solvent, with those observed for polystyrene solutions in toluene and carbon disulfide. In both cases the curves are based on the dilute solution R_g value calculated using eqn (7).

There are no reported SANS measurements of polystyrene/MEK solutions although data for polystyrene over an extended concentration range are available for toluene[33] and carbon disulfide.[34] In both cases the scaling $R_g \propto c^{-\mu}$ continues to high concentration without the appearance of the expected 'concentrated' regime as shown in Fig. 7. Cheng and co-workers[35] have studied another vinyl polymer, poly(methyl methacrylate) in chloroform and observed cross-over behaviour at both low concentration in to the semi-dilute regime and at high

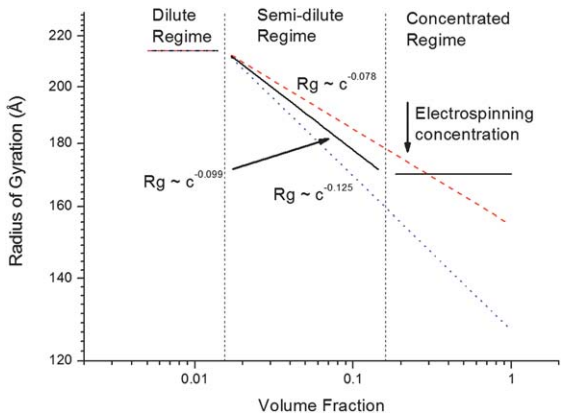

Fig. 7 A plot of R_g against concentration. The solid line is an estimate based on scaling laws for a good solvent.[31] The dashed lines are based on the scaling exponents taken from work on polystyrene solutions in CS_2[34] and toluene.[33]

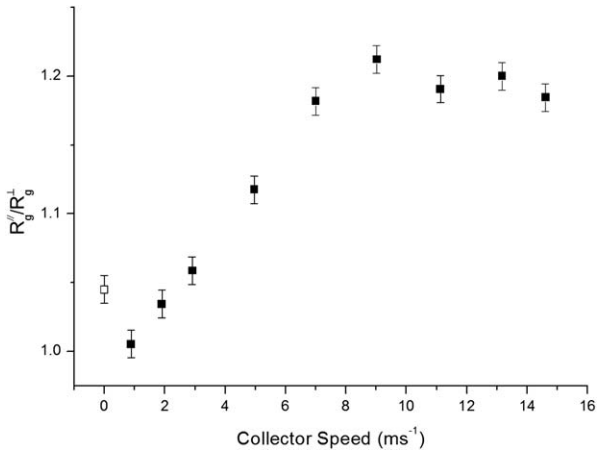

Fig. 8 Ratio of the radius of gyration R_g measured parallel and perpendicular to the rotation direction derived from the data in Fig. 6. The open symbol corresponds to the fibres prepared with the parallel plate electrode system.

concentration in the concentrated regime. This system was selected as it exhibited strong excluded volume effects. The observed cross-over point matched the expected behaviour.[35] Using the same approach but with the molecular parameters appropriate to the polystyrenes used in this work we estimate that the cross-over point to the concentrated regime is 16% v/v (~20% w/w). These cross-over points are shown in Fig. 7. This means that the solution used in this work should be in the concentrated regime. Of course, there will be a variation of the concentration along the electrospinning jet before the collector. All of these localised concentrations will be in the concentrated regime. It should be noted that for fibres collected immediately after spinning, the amount of solvent remaining is ~1% v/v. We await SANS measurements of the radius of gyration of polystyrene in MEK to validate this cross-over estimate. On the basis the cross-over concentration estimated above, we expected that the radius of gyration observed in the electrospun fibres should approach that of the bulk state. The fact that the mean value is ~5% higher may reflect that the semi-dilute scaling regime continues to higher concentrations as observed in polystyrene with toluene as a solvent. This difference in behaviour may be strongly influenced by the dominating effect of the phenyl groups in determining the molecular arrangements in atactic polystyrene.[36]

Fig. 8 shows a plot of the ratio of the radius of gyration parallel to- and perpendicular to- the fibre axis. The results for the fibres collected with static plates and with the rotating collector with tangential velocities of 3 ms^{-1} both give a value of the ratio as ~1.05. In one of these cases the collector is static and in the other the speed of collection more or less matches that of the fibres produced by the electrospinning jet. We conclude that for this system with the defining parameters of the solution, needle and the electric field that there is a limited but finite extension of the polymer chains parallel to the fibre axis which is inherent to the electrospinning process. As the collector speed increases beyond 3–5 ms^{-1} there is a further extension due to mechanical drawing of the polymer chains as a consequence of the fact that the tangential velocity is greater than the velocity of the fibres produced by electrospinning. This effect appears to plateau out for the highest collector speeds explored. It is possible that the relatively low level of anisotropy is the result of averaging over fibres with no anisotropy with a few fibres of high anisotropy. We have examined the fibres using polarised light microscopy and although detailed examination is challenging due to the shape and size of the fibres, these fibres appear to have a reasonably uniform birefringence, indicating a similar level of molecular anisotropy.

We have already indicated that the fibres produced here exhibit a flattened cross-section and the cross-sectional shape and area of the fibres were evaluated by imaging cross-sections taken normal to the fibre axis, an example is shown as the inset in Fig. 9. The ratio of the long axis to the short axis is ~2.5 for all of the fibre samples considered in this work. Koombhongse *et al.* have proposed that this type of cross-section occurs following the formation of a skin which traps some solvent which when it evaporates, the fibre collapses to the flattened structure.[26] Clearly

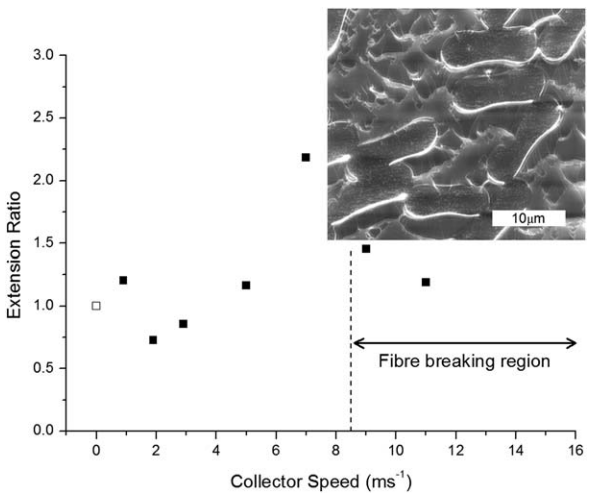

Fig. 9 Calculated extension ratio for fibres prepared with different collector speeds. The inset shows a SEM micrograph of cross-sections of the ribbon like fibres prepared with the static parallel plate electrodes embedded in an epoxy resin.

the processes involved in this transformation are complex but we have formulated a simple geometric model. Consider that the skin formation occurs at a polymer fraction of p which would give a circular cross-section of πr_p^2. If the fibre collapses to a cross-section with a width equivalent to this diameter $2r_p$ and a height h, the aspect ratio $2r_p/h$ is equal to 2.5. The volumetric polymer fraction at the point of the skin formation $p \approx 0.51$ compared with 0.22 in the initial solution.

On the basis that the fibre density remains constant we can use the ratio of the cross-sectional areas of the fibres obtained with the static collector and those obtained with the rotating collector to obtain an effective extension ratio which relates to the mechanical fibre extension imposed by the rotating collector. This extension ratio is plotted against the tangential collector speed in Fig. 9. It can be seen that these calculated macroscopic extension ratios are quite low. There is an initial drop in the apparent extension ratio, as was observed for the levels of fibre orientation discussed earlier and which was attributed to the lack of tension on the fibres. In fact for 2 cross-sections, the calculated extension ratio is slightly less than 1.0 and suggests that on untensioned fibres the model used is too simple. The maximum extension ratio observed before fibre breakage occurs is 2.2 for fibres prepared at tangential speed of $\sim$7 ms^{-1}. The jet breaks near the Taylor cone because this is the weakest part of the jet being rather richer in solvent. A simple model of extension coupled with the speed of the jet evaluated earlier of 4.2 ms^{-1} giving a differential speed of 2.8 ms^{-1} and a needle to electrode distance of 0.2 m gives an estimated macroscopic extension ratio of $\sim$2.3 compared to that estimated *via* the cross-section of 2.2. However, if we now consider the effective molecular extension through the ratio of R_g parallel to the mean isotropic R_g value, this gives a maximum extension ratio of $\sim$1.1 for fibres prepared at a tangential speed of 7 ms^{-1}.

The extent of molecular anisotropy which develops in any extension process depends on both the rate of macroscopic extension and the rate of relaxation. The latter will depend greatly on the molecular weight of the polymer chains and on the concentration of the solution. This will vary throughout the flight to the collector and as a consequence the glass transition will increase until it exceeds the spinning temperature at which point the molecular organisation becomes frozen in the fibre. Relaxation times reported for electrospinning solutions in the literature[37] suggest that relaxation will be dominant and hence high levels of anisotropy are unexpected. The formation of a skin on the fibre during flight which leads to the collapsed rather flat cross-section introduces an additional complication. The formation of such a skin, with a higher viscosity, means that it will carry the stress, allowing the remaining solution to be relatively stress free and therefore nearly isotropic in nature. It is possible that the orientation developed during electrospinning and during the windup is localised in the skin as observed by Tosaka *et al.* with a crystallisable polystyrene.[9] As observed for poly(ε-caprolactone) a small level of induced molecular alignment will lead to a substantial level of crystal orientation.[12] In this study we are able to observe directly this initial low level of molecular alignment.

Fig. 10 shows the orientation parameters $\langle P_2 \rangle$ derived from the SANS data plotted against the estimated extension ratio compared with the predictions of the pseudo affine model and of

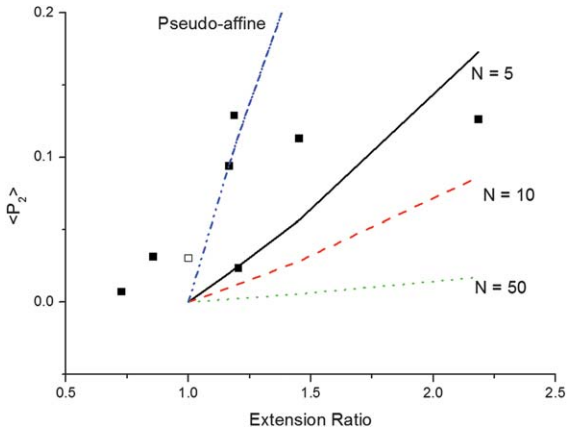

Fig. 10 Values of $\langle P_2 \rangle$ obtained from the SANS data plotted against the calculated extension ratio compared with the prediction for a pseudo-affine model, and for an affine network model with N statistical links.

an affine network with differing number (N) of statistical links between cross-link points.[38] There is limited agreement although the initial development matches the pseudo-affine model as might be expected for deformation taking place in the viscous almost glassy-like skin.

With the data presented, we can start to formulate a more detailed picture of the molecular processes during electrospinning. The initial solution is expected to be in the concentrated regime with $\sim$80% v/v solvent; this provides the required viscoelastic properties required to inhibit beading. The jet thins and the solvent is lost until at $\sim$50% v/v solvent a skin forms which can support the stress. Further solvent loss takes place down to 1% v/v by which time the fibre is at the collector. Throughout the flight, the chains are extended and relaxed at a rate dependent on the temperature and the concentration. Here we need to consider both the relaxation from an extended conformation as well as the relaxation in size from one concentration to another. If we consider the variation of R_g with concentration in Fig. 7 we can see that values obtained in the final electrospun fibres are almost in agreement with the expectations especially if the radius of gyration in solution follows the same scaling with concentration as that observed in the polystyrene/toluene solutions. This would be the last point in the flight of the jet that the chain had adapted or relaxed to the reducing concentration. This appears to be at an earlier point to that predicted for the skin formation. In terms of preferred orientation, the collapse of the fibre at a later point does not affect the orientation as the collapse is largely orthogonal to the fibre axis. It is highly likely that the core of the fibre has a much lower level of anisotropy in terms of the polymer chains than the skin. The final molecular size and shape largely depend on the relaxation behaviour and the size probably reflects a relationship between R_g and concentration for atactic polystyrene and MEK as observed for polystyrene and toluene.

Conclusions

We have obtained high quality SANS data from macroscopically aligned arrays of fibres electrospun from methyl ethyl ketone based solutions. The radius of gyration values of the chains

within the fibre are about 5% greater than that of the bulk value. Measurements parallel and perpendicular to the fibre axis on the sample collected onto the parallel plate arrangement show small signs of anisotropy (~5%) along the fibre axis indicating that the electrospinning process inherently produces anisotropy within the sample. Fibres collected onto the rotating collector show that with an increased collector speed there is a narrowing of the fibre diameter. Along with this narrowing the fibres begin to align more, but after the point where the collector speed matches the jet speed, the fibres are being stretched and deformed. By deforming the sample at high collector speeds this extension can be increased to ~20% along the fibre axis.

Acknowledgements

This work was supported by the EPSRC, the SANS experiments were possible through an award of beam time at the STFC ISIS Facility. The microscopy was carried using facilities in the Centre for Advanced Microscopy and the NMR using the Chemical Analysis Facility at the University of Reading. We thank Drs Richard Heenham and Steve King for their help with the SANS experiments.

References

1 A. Greiner and J. H. Wendorff, *Angew. Chem., Int. Ed.*, 2007, **46**, 5670.
2 K. Yoon, B. S. Hsiao and B. Chu, *J. Mater. Chem.*, 2008, **18**, 5326–5334.
3 M. Stasiak, C. Roben, N. Rosenberger, F. Schleth, A. Studer, A. Greiner and J. H. Wendorff, *Polymer*, 2007, **48**, 5208.
4 C. Wang, K.-W. Yan, Y.-D. Lin and P. C. H. Hsieh, *Macromolecules*, 2010, **43**, 6389.
5 R. Vasita and D. S. Katti, *Int. J. Nanomed.*, 2006, **1**, 15; L. A. Smith, X. Liu and P. X. Ma, *Soft Matter*, 2008, **4**, 2144–2149.
6 G. Taylor, *Proc. R. Soc. London, Ser. A*, 1964, **280**, 383.
7 S. L. Shenoy, W. D. Bates, H. L. Frisch and G. E. Wnek, *Polymer*, 2005, **46**, 3372–3384.
8 D. H. Reneker, A. L. Yarin, H. Fong and S. Koombhongse, *J. Appl. Phys.*, 2000, **87**, 4531.
9 M. Tosaka, K. Yamaguchi and M. Tsuji, *Polymer*, 2010, **51**, 547.
10 L. M. Bellan and H. G. Craighead, *Polymer*, 2008, **49**, 3125–3129.
11 W. A. Yee, A. C. Nguyen, P. S. Lee, M. Kotaki, Y. Liu, B. T. Tan, S. Mhaisalkar and X. Lu, *Polymer*, 2008, **49**, 4196–4203.
12 M. D. Edwards, G. R. Mitchell, S. D. Mohan and R. H. Olley, *Eur. Polym. J.*, 2010, **46**, 1175–1183.
13 Y. Wu, L. A. Carnell and R. L. Clark, *Polymer*, 2007, **48**, 5653–5661.
14 K. H. Lee, K. W. Kim, A. Pesapane, H. Y. Kim and J. F. Rabolt, *Macromolecules*, 2008, **41**, 1494–1498.
15 C. Wang, T.-C. Hsieh and Y.-W. Cheng, *Macromolecules*, 2010, **43**, 9022–9029.
16 S. F. Fennessey and R. J. Farris, *Polymer*, 2004, **45**, 4217–4225.
17 C. Wang, C.-H. Hsu and J.-H. Lin, *Macromolecules*, 2006, **39**, 7662–7672.
18 G. Hadziioannou, L.-H. Wang, R. S. Stein and R. S. Porter, *Macromolecules*, 1982, **15**, 880–882.
19 D. Bradford, B. Hammouda, C. J. Glinka, R. A. Bubeck, J. R. Schroeder and P. Thiyagarajan, *J. Appl. Crystallogr.*, 1990, **23**, 1.
20 F. Boué, M. Nierlich, G. Jannink and R. Ball, *J. Phys. (Paris)*, 1982, **43**, 137.
21 G. D. Wignall and Y. B. Melnichenko, *Rep. Prog. Phys.*, 2005, **68**, 1761–1810.
22 R. K. Heenan, J. Penfold and S. M. King, *J. Appl. Crystallogr.*, 1997, **30**, 1140.
23 R. K. Heenan, S. M. King, R. Osborn and H. B. Stanley, *COLETTE Users Guide*, Rutherford Appleton Laboratory Report RAL-89-128, 1989; S. M. King and R. K. Heenan, *Using COLETTE*, Rutherford Appleton Laboratory Report RAL-95-005, 1995.
24 G. D. Wignall and F. S. Bates, *J. Appl. Crystallogr.*, 1987, **20**, 28.
25 R. K. Heenam, *FISH Reference Manual*, RAL REPORT 89-129, 1989.
26 S. Koombhongse, W. Liu and D. H. Reneker, *J. Polym. Sci., Part B: Polym. Phys.*, 2001, **39**, 2598.
27 R. Lovell and G. R. Mitchell, *Acta Crystallogr., Sect. A: Cryst. Phys., Diffr., Theor. Gen. Crystallogr.*, 1981, **37**, 135–137.
28 G. R. Mitchell, S. Saengsuwan and S. Bualek-Limcharoen, *Prog. Colloid Polym. Sci.*, 2005, **130**, 149–158.
29 T. Kongkhlang, K. Tashiro, M. Kotaki and S. Chirachanchai, *J. Am. Chem. Soc.*, 2008, **130**, 15460–15466.
30 M. Kotlarchyk and S. H. Chen, *J. Chem. Phys.*, 1983, **79**, 2461.
31 M. Daoud and G. Jannink, *J. Phys. Colloq.*, 1976, **37**, 973.
32 M. E. Lewis, S. Nan, W. Yunan, J. Li, J. W. Mays and N. Hadjichristidis, *Macromolecules*, 1991, **24**, 6686–6689.
33 J. S. King, W. Boyer, G. D. Wignall and R. Ullman, *Macromolecules*, 1985, **18**, 709–718.
34 M. Daoud, J. P. Cotton, B. Farnoux, G. Jannink, G. Sarma, H. Benoit, R. Duplessix, C. Picot and P. G. de Gennes, *Macromolecules*, 1975, **8**, 804–818.
35 G. Cheng, W. W. Graessley and Y. B. Melnichenko, *Phys. Rev. Lett.*, 2009, **102**, 157801.
36 G. R. Mitchell and A. H. Windle, *Polymer*, 1984, **25**, 906.
37 T. Han, A. L. Yarin and D. H. Reneker, *Polymer*, 2008, **49**, 1651.
38 G. R. Mitchell, D. J. Brown and A. H. Windle, *Polymer*, 1985, **26**, 1755.

